Article

Molecular tuning of CO$_2$-to-ethylene conversion

Fengwang Li[1,5], Arnaud Thevenon[2,5], Alonso Rosas-Hernández[2,5], Ziyun Wang[1,5], Yilin Li[1,5], Christine M. Gabardo[3], Adnan Ozden[3], Cao Thang Dinh[1], Jun Li[1,3], Yuhang Wang[1], Jonathan P. Edwards[3], Yi Xu[3], Christopher McCallum[3], Lizhi Tao[4], Zhi-Qin Liang[1], Mingchuan Luo[1], Xue Wang[1], Huihui Li[1], Colin P. O'Brien[3], Chih-Shan Tan[1], Dae-Hyun Nam[1], Rafael Quintero-Bermudez[1], Tao-Tao Zhuang[1], Yuguang C. Li[1], Zhiji Han[2], R. David Britt[4], David Sinton[3], Theodor Agapie[2]*, Jonas C. Peters[2]* & Edward H. Sargent[1]*

The electrocatalytic reduction of carbon dioxide, powered by renewable electricity, to produce valuable fuels and feedstocks provides a sustainable and carbon-neutral approach to the storage of energy produced by intermittent renewable sources[1]. However, the highly selective generation of economically desirable products such as ethylene from the carbon dioxide reduction reaction (CO$_2$RR) remains a challenge[2]. Tuning the stabilities of intermediates to favour a desired reaction pathway can improve selectivity[3–5], and this has recently been explored for the reaction on copper by controlling morphology[6], grain boundaries[7], facets[8], oxidation state[9] and dopants[10]. Unfortunately, the Faradaic efficiency for ethylene is still low in neutral media (60 per cent at a partial current density of 7 milliamperes per square centimetre in the best catalyst reported so far[9]), resulting in a low energy efficiency. Here we present a molecular tuning strategy—the functionalization of the surface of electrocatalysts with organic molecules—that stabilizes intermediates for more selective CO$_2$RR to ethylene. Using electrochemical, operando/in situ spectroscopic and computational studies, we investigate the influence of a library of molecules, derived by electro-dimerization of arylpyridiniums[11], adsorbed on copper. We find that the adhered molecules improve the stabilization of an 'atop-bound' CO intermediate (that is, an intermediate bound to a single copper atom), thereby favouring further reduction to ethylene. As a result of this strategy, we report the CO$_2$RR to ethylene with a Faradaic efficiency of 72 per cent at a partial current density of 230 milliamperes per square centimetre in a liquid-electrolyte flow cell in a neutral medium. We report stable ethylene electrosynthesis for 190 hours in a system based on a membrane-electrode assembly that provides a full-cell energy efficiency of 20 per cent. We anticipate that this may be generalized to enable molecular strategies to complement heterogeneous catalysts by stabilizing intermediates through local molecular tuning.

Recently we found that an N-aryl-substituted tetrahydro-4,4′-bipyridine organic thin film, formed by reductive electro-dimerization of an N-aryl pyridinium additive (Fig. 1a; see Supplementary Information for details), facilitated selective CO$_2$RR to multi-carbon products on Cu foils[11]. However, the selectivity and partial current density for ethylene are low (about 40% and 0.5 mA cm^{-2}) for practical applications. We sought to clarify factors contributing to the selectivity enhancement to enable further design of new functional molecules with better performance.

Noting that local environment plays a role in electrocatalysis through tuning interactions among reactants/intermediates[12–16], we postulated that the N-arylpyridinium-derived film may affect the selectivity of CO$_2$RR by interacting with the reaction intermediate(s). To test this hypothesis, we first prepared a library of N-arylpyridinium salts (1–11, Fig. 1b, Supplementary Figs. 1 and 2) expected to display different electronic properties. We then electrodeposited these N-arylpyridinium precursors onto a porous polytetrafluoroethylene gas diffusion layer[17] with a sputtered Cu layer serving as both current collector and catalyst. The as-electrodeposited thin film is water-insoluble and consists of a mixture of both constitutional isomers and stereo isomers of N-aryl-substituted tetrahydro-bipyridine species (Fig. 1a, Supplementary

[1]Department of Electrical and Computer Engineering, University of Toronto, Toronto, Ontario, Canada. [2]Division of Chemistry and Chemical Engineering, California Institute of Technology, Pasadena, CA, USA. [3]Department of Mechanical and Industrial Engineering, University of Toronto, Toronto, Ontario, Canada. [4]Department of Chemistry, University of California, Davis, CA, USA. [5]These authors contributed equally: Fengwang Li, Arnaud Thevenon, Alonso Rosas-Hernández, Ziyun Wang, Yilin Li. *e-mail: agapie@caltech.edu; jpeters@caltech.edu; ted.sargent@utoronto.ca

a

b

c
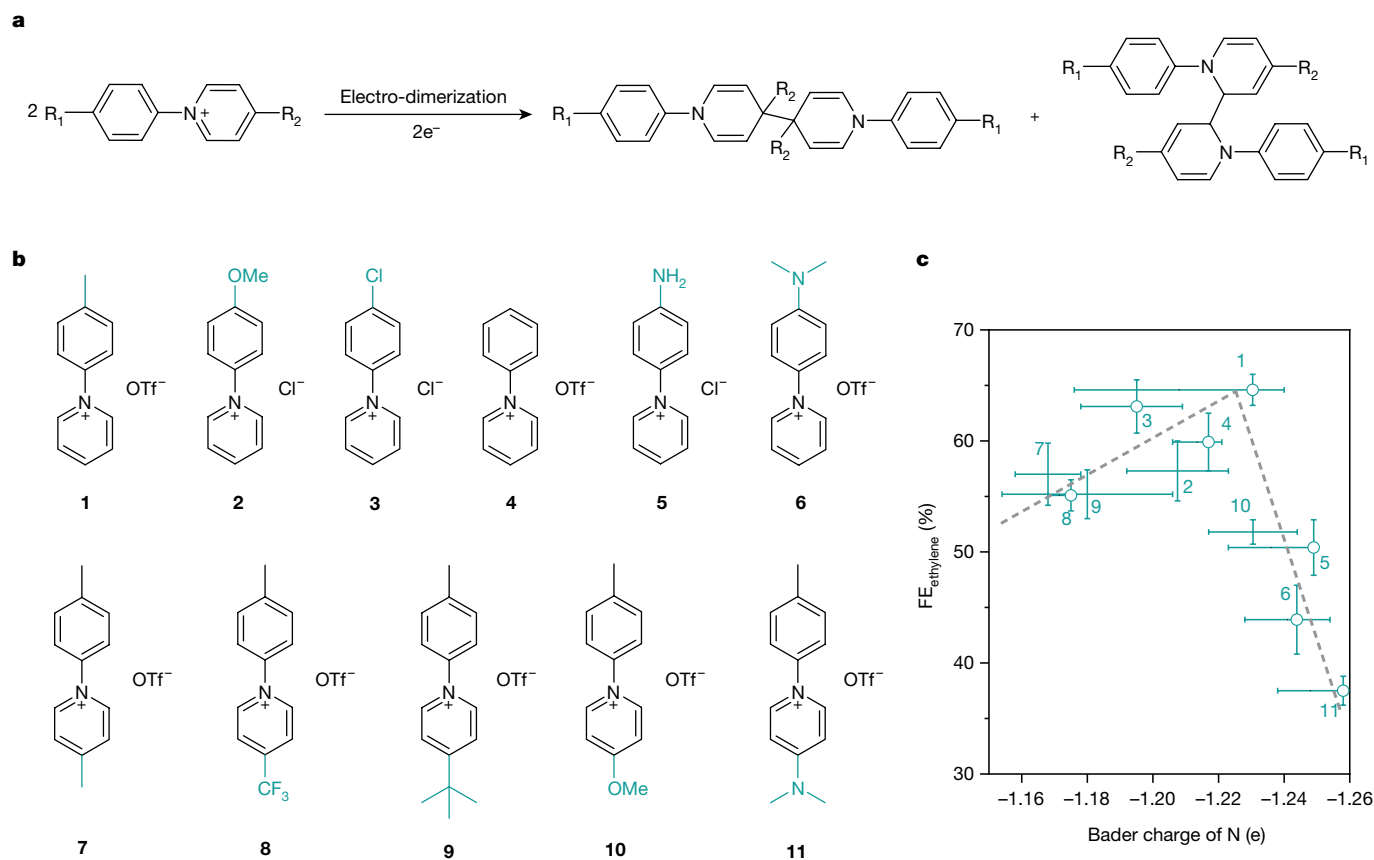
Fig. 1 | Dimerization of *N*-arylpyridinium additives, and correlation of ethylene selectivity with Bader charge. a, Reaction describing the electro-dimerization process that converts an *N*-arylpyridinium salt to a mixture of *N*-aryl-substituted tetrahydro-bipyridines. **b**, Molecular structures of additives **1**–**11**. OTf⁻ is trifluoromethanesulfonate. Cl⁻ and OTf⁻ are the counter-ions of the derivatives. **c**, Trend for ethylene FE and calculated Bader charge for the nitrogen atom of the *N*-aryl-substituted tetrahydro-bipyridines prepared from **1**–**11**. Owing to the symmetric molecular structure of the tetrahydro-bipyridines, a hydrogen atom was used to replace half of the dimer unit (see Supplementary Fig. 6 for details). A spread of Bader charges for the nitrogen,

covering the limiting values of the *para,para* and *ortho,ortho* structures, was plotted. The circles correspond to the average contribution from both the *para,para* and *ortho,ortho* isomers where their ratio could be determined by ¹H NMR spectroscopy (see Supplementary Note 1 for details). The error bars for ethylene FE uncertainty represent one standard deviation based on three independent samples. The corresponding error bars for ethylene FE uncertainty were arbitrarily placed in the middle of the limiting values for those tetrahydro-bipyridines for which the *para,para* versus *ortho,ortho* ratio could not be reliably determined by ¹H NMR spectroscopy.

Note 1, Supplementary Figs. 3–5). As expected, Bader charge analysis points to different electron donating abilities of these tetrahydro-bipyridines (Supplementary Fig. 6). Coating of the tetrahydro-bipyridine film onto the Cu electrode does not substantially change its morphology, crystallinity, electronics or wettability, nor does it retard the transport of reactants, ions and products, which is needed in electrocatalytic processes (Supplementary Note 2, Supplementary Figs. 7–10).

We evaluated CO_2RR properties of these tetrahydro-bipyridine-functionalized electrodes in a liquid-electrolyte flow cell system (Supplementary Fig. 11), using CO_2-saturated 1 M aqueous $KHCO_3$ as the supporting electrolyte. In this system, the abundant catalyst/electrolyte/CO_2 triple-phase interfaces overcome the CO_2 mass-transport limit[17,18] and thus enable commercially relevant current densities[19,20]. We note that, although the large achievable current densities in the flow cell drive up local pH (Supplementary Fig. 12), the tetrahydro-bipyridine layer does not create a further pH gradient near the active Cu surface (Supplementary Note 2). The layer is chemically robust to the locally alkaline environment (Supplementary Fig. 13). The Faradaic efficiency (FE) for ethylene (Supplementary Table 1) on additive-modified Cu−**x** electrodes (**x** = **1**–**11**), at the optimal applied potentials, −0.82 V to −0.84 V versus the reversible hydrogen electrode (RHE; all potentials are with respect to this reference), was plotted against the Bader charge of the nitrogen atom of each tetrahydro-bipyridine structure (Fig. 1c).

We found a volcano-shaped trend relating FE and Bader charge, with the tetrahydro-bipyridine of moderate electron-donating ability showing the highest ethylene selectivity.

We further found a volcano-shaped relationship between the ethylene selectivity and the ratio of atop-bound CO (CO_{atop}) to bridge-bound CO (that is, CO bound to two Cu atoms, hereafter CO_{bridge}) on Cu−**x** surfaces (Fig. 2a). We identified and quantified these bound CO configurations through in situ Raman spectroscopic interrogation[21–24] of these surfaces (Supplementary Note 3, Supplementary Figs. 14 and 15, Supplementary Table 2). In all cases, the ratio of CO_{atop} to CO_{bridge} on Cu−**x** was increased relative to that on bare Cu. Noting a correlation between ethylene selectivity and electron-donation propensity (Fig. 1c), we hypothesized that the change of the relative population of CO_{atop} and CO_{bridge} could arise from the difference in electron-donating abilities of the tetrahydro-bipyridines. Indeed, we found that the ratio of CO_{atop} to CO_{bridge} was positively correlated with the Bader charge of the nitrogen atom in the tetrahydro-bipyridines (Fig. 2b). This finding suggests that electron donation to the *CO stabilizes the atop CO more than it does the bridge CO.

To gain molecular-level insight into the effect of CO binding, we calculated, using density functional theory (DFT), reaction barriers for the CO dimerization step, a critical step along the pathway to C_2 products[5] (that is, products with two carbon atoms, such as ethylene
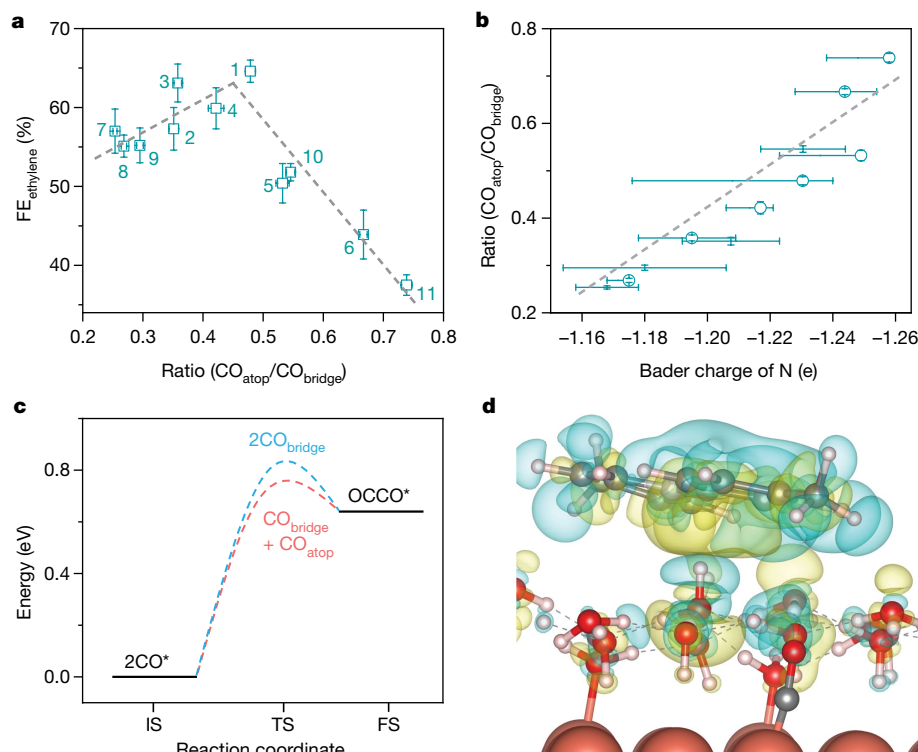
Fig. 2 | Mechanistic investigations of the stabilization of CO-bound intermediates. a, The relationship between the ethylene FE and the ratio of atop CO and bridge CO on Cu–**x** electrodes. The relative population of these two kinds of Cu-bound CO was calculated through the integrated areas of each band in the Raman spectra, which are proportional to the corresponding *CO coverage (see Supplementary Note 3 for more details). The error bars for ethylene FE uncertainty represent one standard deviation based on three independent samples. **b**, The relationship between the ratio of atop CO to bridge CO on Cu–**x** and the Bader charge for the nitrogen atom of the *N*-aryl-substituted tetrahydro-bipyridine formed from additive **x**. The Bader charges

and associated uncertainty were calculated using the same protocol as in Fig. 1. The error bars for the ratio of CO_{atop} to CO_{bridge} in **a** and **b** represent one standard deviation based on two independent measurements. **c**, Energy barriers of the dimerization of two CO at both bridge sites and two CO at bridge and atop sites, respectively. IS, initial state; TS, transient state; FS, final state. **d**, Plots of electron density difference for the CO adsorption with one water layer and the tetrahydro-bipyridine formed from **1**. The yellow and blue contours represent electron density accumulations and depressions, respectively. Dashed lines indicate hydrogen bond network. Red, O; grey, C; blue, N; white, H; pink, Cu.

and ethanol), on Cu(111) with the initial configurations of two *CO on the atop:atop, atop:bridge and bridge:bridge sites (Fig. 2c, Supplementary Fig. 16). We found the lowest barrier of CO dimerization to be at the atop:bridge site with a barrier of 0.72 eV. In comparison, the barrier for the bridge:bridge site is 0.82 eV. The barrier for the atop:atop site could not be identified: one of the CO on atop site tends to relocate to bridge site, suggesting that atop:atop is not favourable for CO dimerization. These findings indicate that neither too large nor too small a population of atop CO favours C_2 selectivity.

We further calculated the adsorption of CO on Cu(111) (Supplementary Fig. 17, Supplementary Table 3). On bare Cu(111), the bridge site appears to be the most stable adsorption site for CO. In the presence of the tetrahydro-bipyridine formed from **1**, the adsorption of CO on both bridge and (especially) atop sites is enhanced, and the atop site becomes favoured compared with the bridge site. The enhancement of CO binding energy decreases the desorption of *CO and increases the likelihood of further reduction of *CO to ethylene (Supplementary Figs. 18–20).

We visualized the interaction between the tetrahydro-bipyridine molecule and *CO through the electron density difference plot (Fig. 2d). The electron density appears to transfer from the molecule to nearby water molecules, changing the electronic distributions of water surrounding *CO, and enhancing CO adsorption in the favourable atop site.

In sum, our working model is that H_2O-mediated electron density transfer of the tetrahydro-bipyridine film to *CO stabilizes this intermediate, especially on the atop site, and therefore promotes the energy-favourable dimerization of bridge:atop bound CO, leading to enhanced

ethylene selectivity. However, too strong an adsorption of CO caused by strong electron donation of some tetrahydro-bipyridines (right side of the volcano plot in Fig. 1c) results in overload of atop-bound CO and thus yields energy barriers too large for further reaction.

We found, by using operando X-ray absorption spectroscopy (XAS, Supplementary Fig. 21), that tetrahydro-bipyridine does not modulate the oxidation state or coordination environment of Cu—although such modulation is known to promote ethylene formation[9,25]. We also found, from in situ electrochemical electron paramagnetic resonance spectroscopic (EPR) and isotopic labelling studies (Supplementary Figs. 22–24), that tetrahydro-bipyridine does not mediate electron transfers via its conversion to pyridinium radicals[16,26], nor does it mediate hydrogen-transfer steps.

Because the nitrogen atom of the *N*-aryl-substituted pyridine ring influences the binding of *CO, we posited that an *N*-aryl-pyridinium-derived molecule with more nitrogen sites and optimal electron-donating properties would stabilize more *CO on the Cu surface. Accordingly, we synthesized an *N,N'*-(1,4-phenylene)bispyridinium salt (**12**, Fig. 3a, Supplementary Fig. 1). In contrast with **1**–**11**, **12** underwent oligomerization to form an *N*-aryl-dihydropyridine-based oligomer under electrodeposition (Fig. 3a, Supplementary Fig. 5). The Bader charge of the nitrogen atom of the oligomer (Supplementary Fig. 6) is close to that of the tetrahydro-bipyridine from **1**, and, as expected, the ratio of CO_{atop} to CO_{bridge} on Cu–**12** (Supplementary Fig. 15, Supplementary Table 2) is also close to that on Cu–**1**. Based on the working hypotheses presented here, these findings suggest the Cu–**12** catalyst should approach the top of the volcano plot.
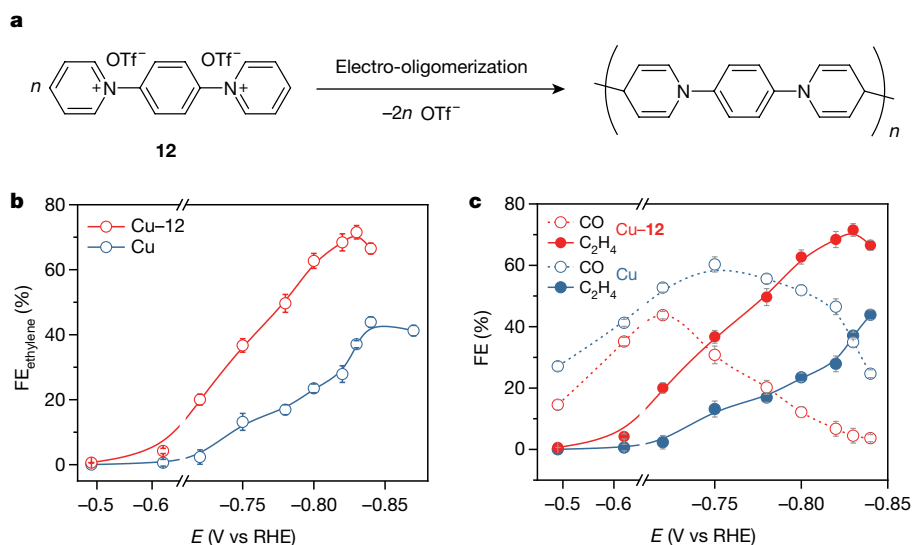
Fig. 3 | CO₂RR performance in liquid-electrolyte flow cells. a, Reaction describing the electro-oligomerization of the *N,N'*-(1,4-phenylene) bispyridinium salt **12** to form an *N*-aryl-dihydropyridine-based oligomer. **b**, FE of ethylene on Cu and Cu–**12** using CO₂-saturated 1 M KHCO₃ as the supporting electrolyte. **c**, FEs of CO and ethylene on Cu and Cu–**12** at the applied potential range of −0.47 V to −0.84 V. The error bars for FE uncertainty represent one standard deviation based on three independent samples.

We evaluated the CO₂RR performance of Cu–**12** in the same flow cell system. The ethylene FE on Cu–**12** is higher than that on bare Cu and other Cu–**x** across the entire applied potential range (−0.49 V to −0.84 V) and achieves a peak value of 72% at −0.83 V (Fig. 3b, Supplementary Tables 1 and 4), higher than previous selectivities reported for ethylene in neutral media (Supplementary Table 5). In contrast, the ethylene FE on bare Cu under similar conditions is below 40%. High selectivity and high current density combine for an ethylene production current of 232 mA cm⁻² at −0.83 V (Supplementary Fig. 25).

We examined the FEs of CO and ethylene across the applied potential range. Although the FE of CO follows the same trend of peaking at moderate potentials, more CO is converted to ethylene on Cu–**12** than on pure Cu (Fig. 3c, Supplementary Table 4). Specifically, at the applied potential of −0.83 V, the FEs of CO and ethylene on Cu–**12** electrode are 5% and 72%, respectively, whereas the values on bare Cu are 35% and 37%, respectively (Supplementary Fig. 25). The FEs of other CO₂RR products remain similar on both catalysts. These findings suggest that the increased ethylene selectivity arises primarily at the expense of CO evolution. This behaviour agrees with the in situ Raman spectroscopy and DFT calculations, where the *CO is well stabilized for ongoing reduction on the molecularly functionalized Cu electrode.

We confirmed by isotopic CO₂ studies (Supplementary Fig. 26) that the products were from CO₂RR.

To evaluate the potential of the Cu–**12** catalyst for practical applications, we integrated it into a membrane–electrode-assembly device (Supplementary Note 4, Supplementary Figs. 27–34) for electrosynthesis of ethylene through the overall reaction:

$$2CO_2 + 2H_2O \rightarrow C_2H_4 + 3O_2 \; ; \; E^\circ = 1.15 \text{ V}$$
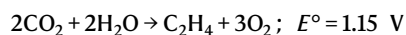
where *E* is the equilibrium potential for the reaction.

We operated the membrane-electrode-assembly system at a full-cell voltage of 3.65 V for 190 h. It exhibited a stable current (approximately 600 mA) and a stable ethylene selectivity (64%) in neutral medium (Fig. 4). The energy efficiency (EE) of the system is determined to be 20% via:

$$EE_{full-cell} = \left(E^\circ \times FE_{ethylene}\right)/E_{full-cell}$$

Overall, this work presents a strategy to tune the stabilization of intermediates on heterogeneous electrocatalysts through the introduction of organic molecules. Using this strategy, implemented with
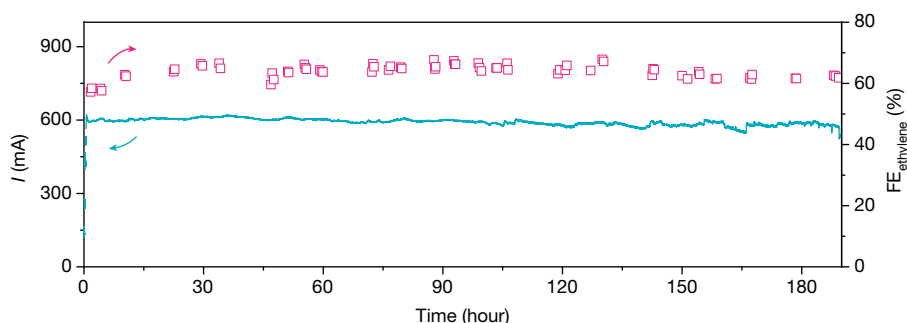
Fig. 4 | Ethylene electrosynthesis in a membrane-electrode assembly device. The operating current and ethylene FE were monitored for the device. Cu–**12** and iridium oxide supported on titanium mesh were used as the cathode and anode, respectively. Humidified CO₂ was flowed through the gas channels in the cathode, and 0.1 M aqueous KHCO₃ solution was flowed through channels in the anode. The anode and cathode were separated by an anion exchange membrane to form the membrane-electrode assembly. The total geometric area of the flow field in the cathode is 5 cm², of which 45% is the gas channel while the remaining 55% is the land area (Supplementary Figs. 27 and 28). Full-cell voltage was gradually increased from 3 V to 3.65 V and kept constant starting at time 0.

N-aryl-substituted tetrahydro-bipyridine films and a related oligomeric film on a Cu catalyst, we achieved CO_2-to-ethylene conversion with an ethylene FE of 72% and a full-cell energy efficiency of 20% in neutral media. In light of this performance, in combination with the long-term operating stability, this is a promising strategy for the use of renewable electricity to convert CO_2 into value-added chemicals, thus storing the renewable energy (solar, wind) in the form of chemical energy.

Online content

Any methods, additional references, Nature Research reporting summaries, source data, extended data, supplementary information, acknowledgements, peer review information; details of author contributions and competing interests; and statements of data and code availability are available at https://doi.org/10.1038/s41586-019-1782-2.

1. Seh, Z. W. et al. Combining theory and experiment in electrocatalysis: insights into materials design. *Science* **355**, eaad4998 (2017).
2. De Luna, P. et al. What would it take for renewably powered electrosynthesis to displace petrochemical processes? *Science* **364**, eaav3506 (2019).
3. Li, Y. & Sun, Q. Recent advances in breaking scaling relations for effective electrochemical conversion of CO_2. *Adv. Energy Mater*. **6**, 1600463 (2016).
4. Calle-Vallejo, F. & Koper, M. T. Theoretical considerations on the electroreduction of CO to C_2 species on Cu(100) electrodes. *Angew. Chem. Int. Ed*. **52**, 7282–7285 (2013).
5. Montoya, J. H., Shi, C., Chan, K. & Nørskov, J. K. Theoretical insights into a CO dimerization mechanism in CO_2 electroreduction. *J. Phys. Chem. Lett*. **6**, 2032–2037 (2015).
6. Yang, K. D. et al. Morphology-directed selective production of ethylene or ethane from CO_2 on a Cu mesopore electrode. *Angew. Chem. Int. Ed*. **56**, 796–800 (2017).
7. Li, C. W., Ciston, J. & Kanan, M. W. Electroreduction of carbon monoxide to liquid fuel on oxide-derived nanocrystalline copper. *Nature* **508**, 504–507 (2014).
8. Jiang, K. et al. Metal ion cycling of Cu foil for selective C–C coupling in electrochemical CO_2 reduction. *Nat. Catal*. **1**, 111–119 (2018).
9. Mistry, H. et al. Highly selective plasma-activated copper catalysts for carbon dioxide reduction to ethylene. *Nat. Commun*. **7**, 12123 (2016).
10. Zhou, Y. et al. Dopant-induced electron localization drives CO_2 reduction to C_2 hydrocarbons. *Nat. Chem*. **10**, 974–980 (2018).
11. Han, Z., Kortlever, R., Chen, H. Y., Peters, J. C. & Agapie, T. CO_2 reduction selective for $C_{\geq 2}$ products on polycrystalline copper with N-substituted pyridinium additives. *ACS Cent. Sci*. **3**, 853–859 (2017).
12. Rosen, B. A. et al. Ionic liquid-mediated selective conversion of CO_2 to CO at low overpotentials. *Science* **334**, 643–644 (2011).
13. Masel, R. I. & Rosen, B. A. Catalyst mixtures. US patent 8,956,990 (2015).
14. Masel, R. I. & Rosen, B. A. Electrochemical devices comprising novel catalyst mixtures. US patent 9,464,359 (2016).
15. Masel, R. I. & Rosen, B. A. Catalyst mixtures. US patent 9,566,574 (2017).
16. Barton Cole, E. et al. Using a one-electron shuttle for the multielectron reduction of CO_2 to methanol: kinetic, mechanistic, and structural insights. *J. Am. Chem. Soc*. **132**, 11539–11551 (2010).
17. Dinh, C.-T. et al. CO_2 electroreduction to ethylene via hydroxide-mediated copper catalysis at an abrupt interface. *Science* **360**, 783–787 (2018).
18. Li, J. et al. Efficient electrocatalytic CO_2 reduction on a three-phase interface. *Nat. Catal*. **1**, 592–600 (2018).
19. Ma, S. et al. One-step electrosynthesis of ethylene and ethanol from CO_2 in an alkaline electrolyzer. *J. Power Sources* **301**, 219–228 (2016).
20. Jouny, M., Luc, W. W. & Jiao, F. General techno-economic analysis of CO_2 electrolysis systems. *Ind. Eng. Chem. Res*. **57**, 2165–2177 (2018).
21. Sheppard, N. & Nguyen, T. T. in *Advances in Infrared and Raman Spectroscopy* Vol. 5 (eds Hawes Clark, R. J. & Hester, R. E.) 67 (Heyden, 1978).
22. Gunathunge, C. M. et al. Spectroscopic observation of reversible surface reconstruction of copper electrodes under CO_2 reduction. *J. Phys. Chem. C* **121**, 12337–12344 (2017).
23. Heyes, J., Dunwell, M. & Xu, B. CO_2 reduction on Cu at low overpotentials with surface-enhanced in situ spectroscopy. *J. Phys. Chem. C* **120**, 17334–17341 (2016).
24. Akemann, W. & Otto, A. Vibrational modes of CO adsorbed on disordered copper films. *J. Raman Spectrosc*. **22**, 797–803 (1991).
25. Xiao, H., Goddard, W. A., Cheng, T. & Liu, Y. Cu metal embedded in oxidized matrix catalyst to promote CO_2 activation and CO dimerization for electrochemical reduction of CO_2. *Proc. Natl Acad. Sci. USA* **114**, 6685–6688 (2017).
26. Cole, E. B., Sivasankar, N., Parajuli, R. & Keets, K. A. Reducing carbon dioxide to products. US patent 8,845,878 (2014).

Article

Data availability

The datasets generated during and/or analysed during the current study are available from the corresponding author on reasonable request.

Author contributions E.H.S., T.A. and J.C.P. supervised this project. F.L. and Y.L. carried out electrochemical experiments. A.T. and A.R.-H. carried out molecule synthesis and characterizations. Z.W. carried out DFT calculations. C.M.G. and F.L. conducted in situ Raman measurement. F.L. and A.O. carried out the membrane–electrode-assembly experiments. J.L. and F.L. performed XAS measurements. Y.W. carried out scanning electron microscopy and electrochemical impedance spectroscopy measurements. J.P.E. measured the contact angle. C.M. carried out the Comsol modelling. L.T. carried out EPR measurement under the supervision of R.D.B. M.L. performed part of the electrochemical experiments. Z.-Q.L., X.W. and H.L. provided help in NMR analysis. C.M.G., C.P.O. and Y.X. provided help in membrane-electrode assembly measurements. C.-S.T. carried out AFM measurement. D.-H.N. conducted X-ray diffraction measurement. R.Q.-B. carried out X-ray photoelectron spectroscopy measurement. C.T.D., T.T.Z., Y.C.L. and Z.H. provided help in materials synthesis and characterizations. F.L. and E.H.S. wrote the manuscript. All authors discussed the results and assisted during manuscript preparation.

Competing interests The authors declare no competing interests.

Additional information
Supplementary information is available for this paper at https://doi.org/10.1038/s41586-019-1782-2.
Correspondence and requests for materials should be addressed to T.A., J.C.P. or E.H.S.
Peer review information *Nature* thanks Muhyun Baik, Richard I. Masel and the other, anonymous, reviewer(s) for their contribution to the peer review of this work.
Reprints and permissions information is available at http://www.nature.com/reprints.